Letter

Three-photon Rydberg-atom-based radio-frequency sensing scheme with narrow linewidth

Stephanie M. Bohaichuk [1,*] Fabian Ripka,[1] Vijin Venu,[1] Florian Christaller,[1] Chang Liu,[1]
Matthias Schmidt,[1] Harald Kübler,[1,2] and James P. Shaffer[1,†]

[1] *Quantum Valley Ideas Laboratories, 485 Wes Graham Way, Waterloo, Ontario N2L 0A7, Canada*

[2] *5. Physikalisches Institut, Universität Stuttgart, Pfaffenwaldring 57, 70569 Stuttgart, Germany*

We demonstrate Rydberg atom-based radio-frequency sensing with a colinear three-photon scheme in a room-temperature cesium vapor cell that minimizes residual Doppler broadening of the probe-laser absorption feature. A sub-200-kHz spectral linewidth is observed and extends the self-calibrated Autler-Townes sensing regime to weaker fields by a factor of 18 compared to the theoretical limit of the most commonly used two-photon scheme. The sensitivity of the method to microsecond pulses is shown to be sufficient to detect radio-frequency Rabi frequencies of $2\pi \times 0.44$ MHz using a 480-kHz bandwidth at 108.9 GHz, demonstrating the ability to sense time-dependent signals suitable for radar and communications.

Calibration is a crucial process for a variety of technologies relying on rf electromagnetic fields, including those in communications, radar, health care, remote sensing, and nondestructive testing. However, absolute rf electromagnetic field measurements have relatively low accuracy and are costly, since they have to be traced back to a standard. Alternative approaches using Rydberg atoms in atomic vapors [1–4] are promising with the potential to complement, and even displace, conventional calibrated rf antennas for test and measurement across a broad frequency range spanning MHz–THz. Atom-based rf electric field (*E*-field) amplitude sensing can be self-calibrated because measurements can be traced to precisely determined atomic structure and fundamental constants [1,2]. These sensors are also electromagnetically transparent, portable, and robust.

In atom-based rf metrology, electromagnetically induced transparency (EIT) or electromagnetically induced absorption (EIA) is altered by an external rf *E* field that is (near) resonant with atomic Rydberg transitions [2,5–8]. The smallest measurable rf *E* field in the self-calibrated Autler-Townes regime, which relies on splitting of the EIT or EIA feature, is set by the spectral linewidth of the optical absorption features. Almost all Rydberg atom-based sensing to date is based on two-photon schemes. For cesium-based sensors, counterpropagating 852-nm probe and 509-nm coupling lasers are used. The spectral linewidth is limited by residual Doppler broadening, arising from the

wave-vector mismatch between these two lasers. For orientationally averaged transition dipole moments, the spectral resolution is limited to $2\pi \times 3.5$ MHz [9]. Optical pumping can slightly improve the spectral resolution [10]. In the amplitude regime, which uses resonant absorption changes to sense weaker rf *E* fields, two-photon schemes can detect rf *E*-field strengths below 1 μV/cm [10,11], with a discussion of fundamental limits found in Refs. [2,12]. Weaker rf *E* fields have been measured using an auxiliary rf *E* field in a heterodyne measurement [13,14]. Rydberg atom-based sensors can detect modulated rf *E* fields, including submicrosecond pulses [15–20]. The sensitivity depends on the transition dipole moment and the sensing geometry.

In this work, we demonstrate a three-photon sensing scheme in a room-temperature (22 °C) cesium vapor cell. A colinear 895-, 636-, and 2262-nm laser geometry is used to sense 108.9-GHz rf *E* fields. The residual Doppler broadening is reduced, approaching a theoretical limit of $2\pi \times 51$ kHz. The wave vectors of the two longer wavelength laser fields are matched to compensate the Doppler shifts of the 636-nm laser field [9,21]. The colinear geometry is advantageous in its straightforward alignment and large interaction volume for fixed laser powers. We achieve a $2\pi \times 190$ kHz experimental spectral linewidth. We theoretically examine the practical limits to the spectral linewidth and show that it is no longer dominated by Doppler broadening. The narrow spectral linewidth significantly extends the self-calibrated Autler-Townes regime, allowing us to resolve spectral splittings of $<2\pi \times 400$ kHz. The improvement is nearly 20 times the

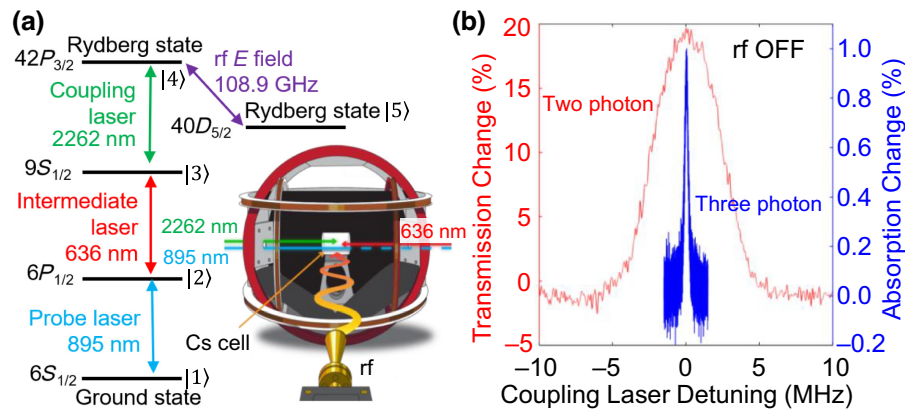*sbohaichuk@qvil.ca
†jshaffer@qvil.ca

FIG. 1. (a) Energy-level diagram and experimental setup. An rf E field is emitted by a horn antenna perpendicular to the optical axis, and is sensed by monitoring the probe laser's transmission through the vapor cell. (b) The absorption feature produced by the three-photon excitation is spectrally narrower by over an order of magnitude relative to a standard two-photon 509- and 852-nm excitation scheme. Rabi frequencies of $\Omega_{895} = 2\pi \times 0.6$ MHz, $\Omega_{636} = 2\pi \times 4.9$ MHz, and $\Omega_{2262} = 2\pi \times 0.17$ MHz with 1.2, 1.3, and 1.7 mm beam diameters are used for the three-photon excitation, while $\Omega_{852} = 2\pi \times 1.7$ MHz and $\Omega_{509} = 2\pi \times 2.1$ MHz with 300-μm beam diameters in a 3-cm-long cell are used for the two-photon excitation.

orientationally averaged, theoretical limit, which is rarely achieved in Rydberg atom-based sensing experiments. We also demonstrate sensing of individual 1–10 μs pulses using a matched filtering technique [20] and measure rf E fields down to fields of approximately 858 μV/cm in a 480-kHz detection bandwidth. The results are superior to prior all-optical two-photon sensing schemes and comparable to current heterodyning experiments at this detection bandwidth, geometry, and rf transition dipole moment.

The experimental setup is shown in Fig. 1(a). Three optical excitation beams pass colinearly through a 2.5-cm cesium vapor cell. Compensation coils are placed around the vapor cell to cancel the background magnetic field, which broadens the spectral line. The 895-nm probe laser drives the $6S_{1/2}(F = 4) \rightarrow 6P_{1/2}(F = 3)$ transition, the 636-nm intermediate coupling beam drives the $6P_{1/2}(F = 3) \rightarrow 9S_{1/2}(F = 4)$ transition, and the 2262-nm Rydberg coupling beam drives the $9S_{1/2}(F = 4) \rightarrow 42P_{3/2}$ transition. The 636-nm beam counterpropagates with the 895- and 2262-nm beams. All beams are circularly polarized. The $1/e^2$ beam diameters of the 895-, 636-, and 2262-nm lasers are 1.2, 1.1, and 1.3 mm, respectively, for narrow linewidth measurements. All the lasers are frequency stabilized to an ultralow expansion cavity using the Pound-Drever-Hall technique. The spectral linewidths of the 895-, 636-, and 2262-nm lasers are estimated to be below $2\pi \times 10$ kHz, $2\pi \times 50$ kHz, and $2\pi \times 50$ kHz, respectively. Changes in the probe beam absorption are detected using an avalanche photodiode with a 10-MHz bandwidth.

A 108.9-GHz rf E field is used to resonantly drive the $42P_{3/2} \rightarrow 40D_{5/2}$ atomic transition. The rf E-field strength is adjusted by a variable attenuator and radiated by a microwave horn antenna placed approximately 15 cm from

the vapor cell. The rf E field propagates perpendicular to the laser beams with the electric field vertically polarized. For this Rydberg transition, the radial dipole matrix element is $632ea_0$ and we use the orientationally averaged dipole moment $\mu = 400ea_0$ for estimating the rf E field.

A spectral line shape with optimized laser locks for the three-photon readout using probe absorption is shown in Fig. 1(b). The three-photon excitation creates EIA, which exhibits an approximately Lorentzian shape with a $2\pi \times 279$ kHz FWHM. For comparison, the transmission line shape obtained in a standard two-photon setup for cesium using counterpropagating 509-nm coupling and 852-nm probe lasers is also shown. Under narrow linewidth conditions, the two-photon system shows a Gaussian shape with a FWHM of approximately $2\pi \times 5$ MHz, over 15× larger than the three-photon system shown in Fig. 1(b). The fact that the spectral line shape for the three-photon readout is Lorentzian demonstrates that it is no longer dominated by the Doppler effect.

Figure 2(a) shows the shape and linewidth of the three-photon signal at different Rabi frequencies, Ω_{636}. The 2262-nm laser is modulated at 61 kHz using an acousto-optic modulator (AOM). The probe-laser transmission is processed with a lock-in amplifier. The asymmetry in the line shape is due to slight misalignment or detuning of the laser beams. The EIA is more sensitive to these effects at weaker Ω_{636}. As Ω_{636} decreases, the signal amplitude decreases and the linewidth reduces to $2\pi \times 190$ kHz at $\Omega_{636} = 2\pi \times 1.7$ MHz, which is 18 times smaller than the orientationally averaged residual Doppler limit of a two-photon system.

To investigate the theoretical spectral linewidth, we performed density-matrix calculations shown in Fig. 2(b). The master equation is solved for the steady-state
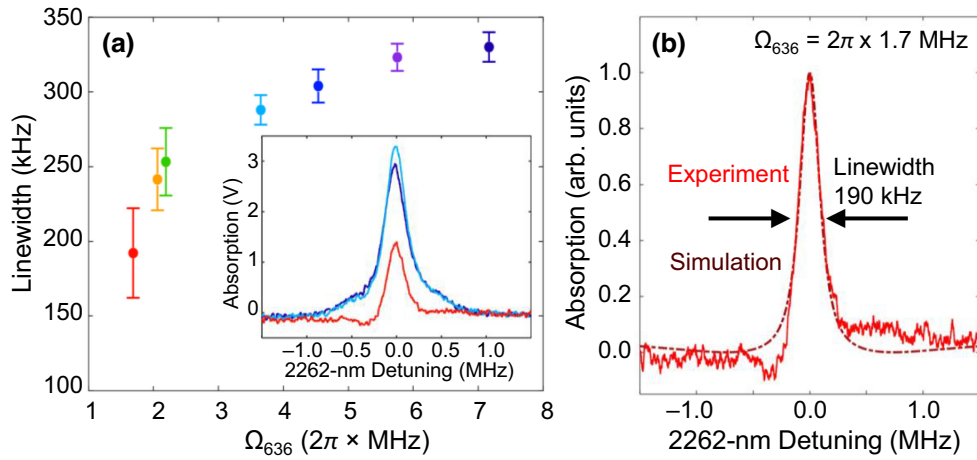
FIG. 2. (a) Extracted Lorentzian linewidth (FWHM) of the three-photon signal with no rf E field present, measured at various intermediate coupling Rabi frequencies Ω_{636}. Error bars represent one standard deviation in the distribution of linewidths from individual traces. The inset shows averaged experimental spectral line shapes. (b) Probe absorption of the three-photon system simulated using a density-matrix model (dot-dashed line), producing a theoretical Lorentzian linewidth of 190 kHz that is comparable to experiment (solid line). $\Omega_{895} = 2\pi \times 1.0$ MHz and $\Omega_{2262} = 2\pi \times 0.04$ MHz.

density matrix in the five-level ladder system in Fig. 1(a) and then thermally averaged (see Supplemental Material [22]). We include radiative and blackbody decay rates in the Lindblad operator for each state: $\Gamma_{21} = 2\pi \times 4.5$ MHz, $\Gamma_{32} = 2\pi \times 200$ kHz, and $\Gamma_{42} = 2\pi \times 2$ kHz [23]. We include a $2\pi \times 110$ kHz transit time broadening. Dephasing terms for each transition are also included based on the sum of the spectral linewidths of the lasers that interact with each level, $\Gamma_{11} = 2\pi \times 10$ kHz, $\Gamma_{22} = 2\pi \times 60$ kHz, $\Gamma_{33} = 2\pi \times 100$ kHz, and $\Gamma_{44} = 2\pi \times 50$ kHz.

In our model, we find that the spectral line shape of the probe absorption is Lorentzian with a FWHM of approximately $2\pi \times 190$ kHz at $\Omega_{895} = 2\pi \times 1.0$ MHz, $\Omega_{636} = 2\pi \times 1.7$ MHz, and $\Omega_{2262} = 2\pi \times 0.04$ MHz, similar to the experimental linewidth under these conditions. Residual Doppler broadening is no longer the limiting factor in the spectral resolution of the Autler-Townes regime, but is one of several contributions to the linewidth, including laser linewidths, Rydberg state lifetimes, and transit time broadening. The fact that the observed EIA line shape is predominantly Lorentzian rather than Gaussian demonstrates this change. Under our experimental conditions the model predicts a low Rydberg state population of $\rho_{44} \sim 3 \times 10^{-5}$ and we do not expect collisions to play a significant role (see Supplemental Material) [22,24]. When the laser linewidths are smaller, <1 kHz, transit time broadening and residual Doppler effects dominate and the three-photon linewidth reduces to 145 kHz. The spectral linewidth is ultimately limited by Rydberg state decay rates and the residual Doppler broadening.

Figure 3 shows experimental probe absorption with a 108.9-GHz continuous-wave rf E field applied. rf E-field amplitude E is determined directly from the self-calibrated

atomic response by fitting a pair of Lorentzians to the absorption peaks and extracting the frequency splitting $\Delta\nu$. This is converted to an rf E-field amplitude using $E = h\Delta\nu/\mu$. As progressively weaker rf E fields are applied, the two peaks begin to overlap until they become indistinguishable at a splitting of approximately $2\pi \times 380$ kHz, corresponding to a field of approximately 745 µV/cm. The data in Fig. 3 demonstrates that the minimum detectable rf E-field amplitude that can be measured in the self-calibrated Autler-Townes regime is reduced by a factor of approximately 9 beyond the smallest reported Autler-Townes field measured in any two-photon setup, at an equivalent dipole moment and as much as 18 fold better than schemes that do not exploit optical pumping [8].

The sensitivity of the three-photon method for measuring weak rf E fields in the amplitude regime relies on detecting small changes in absorption. Sensitivity refers to the minimum rf E field detectable by the sensor within a measurement bandwidth B, usually specified as $E_{min}/\sqrt{B}$. The minimum is defined by the point at which the change in probe-laser absorption induced by the rf E field, relative to the absorption without rf present, approaches noise fluctuations. Better sensitivity is achieved with higher intermediate and Rydberg coupling Rabi frequencies than in the Autler-Townes regime. To increase the Rabi frequency of the Rydberg coupling laser, whose power was limited, we amplified it by seeding a broadband multimode laser diode [25]. We also reduced the 2262-nm laser's beam size to a diameter of approximately 150 µm. The 895-nm laser-beam diameter was reduced to 240 µm to minimize the nonsignal-carrying component of the probe beam. We chose maximum 2262- and 636-nm laser powers, and an optimal power for the 895-nm laser, such
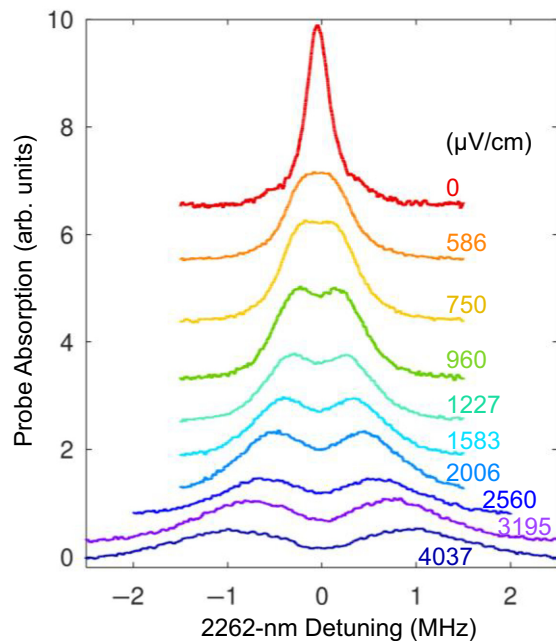
FIG. 3. Autler-Townes splitting of the probe-laser absorption in the vapor cell in response to a 108.9-GHz continuous-wave rf E field whose amplitude is increased from top to bottom. The top trace is measured without an rf E field applied, and produces a FWHM of $2\pi \times 284$ kHz. The self-calibrated rf field strength measured from the atoms via the peak splitting is labeled next to each trace. $\Omega_{895} = 2\pi \times 1.0$ MHz, $\Omega_{636} = 2\pi \times 7.2$ MHz, and $\Omega_{2262} = 2\pi \times 0.04$ MHz.

that rf sensitivity was maximized. This choice is consistent with both experiment and modeling (see Supplemental Material [22]).

We measure the rf E-field sensitivity at $\Omega_{2262} = 2\pi \times 2.4$ MHz, $\Omega_{636} = 2\pi \times 7.2$ MHz, and $\Omega_{895} = 2\pi \times 1.9$ MHz, resulting in a linewidth of approximately $2\pi \times 1.5$ MHz. rf E-field strength is adjusted by a linear attenuator, which is calibrated at high fields where Autler-Townes splitting can be measured. Calibration is performed with the rf E field on resonance, but a slightly higher rf E-field sensitivity is found at an rf E-field detuning of -125 kHz with the 2262 nm detuned by about half that in the opposite direction, most likely due to ac Stark shifts and slight beam misalignment. To measure the sensitivity to individual rf E-field pulses, all lasers are frequency locked, and the rf E field is pulse modulated on a microsecond time scale. To further increase sensitivity and stabilize the atomic density, we heat the vapor cell to 29 °C. We enclose the vapor cell in a small plastic holder containing four resistive microheaters (approximately 2×2 mm²) in contact with the outer corners of the cell, aimed at maintaining rf transparency.

To improve the signal-to-noise ratio and obtain the sensitivity in an operational mode that is closer to the anticipated one in a fieldable device, we make use of a

digital matched filter [20,26]. Matched filtering searches noisy data for periods of strong correlation with a known pulse template via convolution, identifying pulses that are embedded in white noise. For a nearly square pulse, the matched filter has a well-defined detection bandwidth of $B = 1/\tau$, where τ is the pulse duration. For the matched filter's template we use an averaged experimental atomic response, Fig. 4(a) inset [22]. Responses exhibit rapid rise and fall times around 0.5 µs due to the small beam size, i.e., rapid transit time. Typical output from the matched filter is shown in Fig. 4(a), which produces a peak at the time of maximum cross-correlation with the template. We take statistics of the peak of the matched filter in the expected arrival window, minus the average peak noise amplitude when no rf is applied, to produce Fig. 4(b).

We extract a sensitivity for our detection scheme by considering the weakest measurable field to be one at which the average signal height is 1σ above the filtered noise. We perform least-squares fitting of the data at weak fields in the amplitude regime, <2450 µV/cm, where the absorption change is approximately quadratic as a function of rf E-field amplitude [27]. The point at which the curve intersects the upper error bar of the noise distribution when no rf E field is present yields a minimum detectable field for 2-µs pulses of 1225 µV/cm, or $\Omega_{rf} = 2\pi \times 0.63$ MHz. The measurement bandwidth is 500 kHz. Similarly, weaker pulses, down to 955 µV/cm, are measurable at 10-µs pulse durations (100-kHz bandwidth) due to higher total energy in the pulse, while 1754-µV/cm fields can be measured at 1.25-µs pulse durations (800-kHz bandwidth). Our overall best response to short-pulsed rf E fields was obtained at 2.1-µs pulse durations, reaching down to 858 µV/cm, or a Rabi frequency of $2\pi \times 0.44$ MHz, at a detection bandwidth of 480 kHz.

The sensitivity near these measurement bandwidths corresponds to approximately 1.25 µV cm⁻¹ Hz⁻¹/². Due to the nonlinear scaling of absorption with rf E-field amplitude, this value should not be extrapolated to long integration times. Evaluating the sensitivity in terms of minimum detectable rf Rabi frequency rather than rf amplitude allows for a better comparison of technical noise levels because it is independent of the transition dipole moment. For similar pulse durations, measurement bandwidths, and geometry in a two-photon setup with a matched filter, a corresponding Rabi frequency of $2\pi \times 1.37$ MHz was measured [20]. State-of-the-art heterodyne experiments have not been demonstrated at these bandwidths, but can reach minimum Rabi frequencies on the order of $2\pi \times 0.075$ MHz when extrapolated to a 500-kHz bandwidth [13,14]. We note that the heterodyne experiments that have reported these values use over 200 times the atoms, 200 times the probe-laser power, and 14 times less transit time broadening than the experiment reported here. The colinear three-photon approach can therefore offer similar or better pulse sensitivity, $2\pi \times 0.44$ MHz, in the
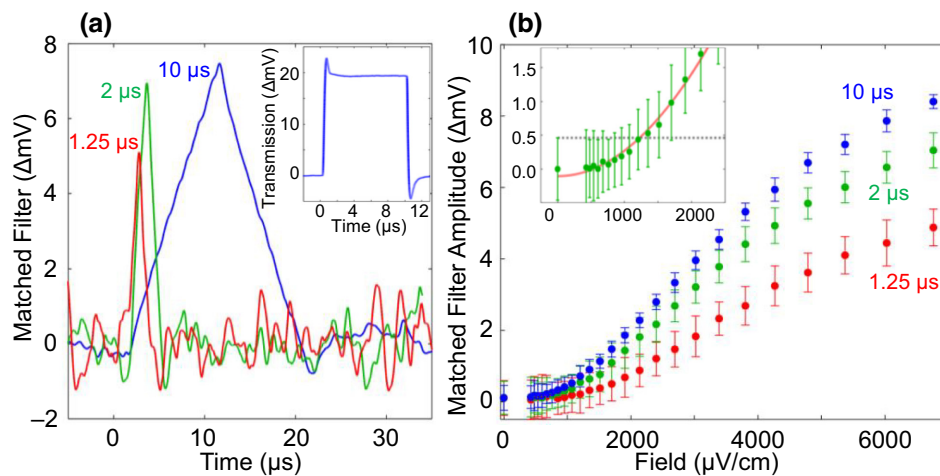
FIG. 4.   (a) Matched filter output in response to single 5365-µV/cm rf pulses. The inset shows an averaged atomic response to a 3724-µV/cm rf pulse, used as a filter template. (b) Average signal height output by the matched filter in response to individual pulses at different rf E-field strengths and pulse durations. The error bars represent one standard deviation from 200–400 pulses. The inset shows a fit (red) to the quadratic amplitude regime at weak rf E fields. Sensitivity is determined by the minimum field at which the average signal height exceeds a 1σ noise error bar (black dashed line in inset) at the measurement bandwidth.

amplitude regime than a two-photon setup, and, even given the differences in geometric conditions, is within an order of magnitude of the quoted heterodyne results.

Large improvements in rf E-field sensitivity can be expected by increasing both the 636- and 2262-nm Rabi frequencies, as well as by using larger beam sizes to decrease transit time broadening and increase the overall probe-laser power for a fixed Rabi frequency. Larger probe-laser powers reduce the photon shot-noise-limited lowest detectable rf E field, while our density-matrix calculations indicate that the optimum sensing point lies at larger 636- and 2262-nm Rabi frequencies. Using larger laser beams also increases the number of atoms and therefore signal. We estimate conservatively that gains of over 30 in sensitivity are achievable by optimizing the coupling laser Rabi frequencies and increasing the beam diameters by a factor of 10 while maintaining the probe-laser Rabi frequency. A downside of increasing the laser-beam size is that the reduced transit time broadening will increase the time it takes for a pulse to reach its final amplitude [20]. Given the narrow linewidth of the rf-induced changes to EIA [22], the three-photon setup is very sensitive to the frequency noise of all three lasers, since frequency noise is converted to signal amplitude noise. While our system is estimated to be within an order of magnitude of the probe-laser photon shot-noise limit, obtaining narrower linewidth lasers, either through laser design or improved frequency locking, is expected to allow the system to reach the probe-laser shot-noise limit. With these improvements, we expect the three-photon system to be comparable to or surpass current state-of-the-art heterodyne results in two-photon systems and potentially surpass the thermal noise limit.

We experimentally demonstrated a colinear three-photon scheme for Rydberg atom-based rf electrometry. The scheme minimizes wave-vector mismatch between the lasers, greatly reducing residual Doppler broadening. We achieve $2\pi \times 190$ kHz EIA spectral linewidths, limited by transit time broadening, spontaneous decay, and laser linewidths. The spectral linewidth is over 18 times narrower than a standard two-photon excitation scheme, and enables measurement of weaker rf E fields within the Autler-Townes regime. Using a matched filter tailored to the atomic response, we measured a minimum rf Rabi frequency of $2\pi \times 0.44$ MHz at a bandwidth of 480 kHz, at 108.9 GHz. At these bandwidths, the minimum Rabi frequency compares well with state-of-the art experiments when geometry and dipole moment are accounted for. We find that higher coupling laser Rabi frequencies and larger beam sizes are beneficial for achieving the highest sensitivity. The narrow linewidth extends the self-calibrated sensing regime to weaker fields, while providing high sensitivity to single rf pulses.

[1] J. A. Sedlacek, A. Schwettmann, H. Kübler, R. Löw, T. Pfau, and J. P. Shaffer, Microwave electrometry with Rydberg atoms in a vapour cell using bright atomic resonances, Nat. Phys. **8**, 819 (2012).

[2] H. Fan, S. Kumar, J. Sedlacek, H. Kübler, S. Karimkashi, and J. P. Shaffer, Atom based RF electric field sensing, J. Phys. B: At. Mol. Opt. Phys. **48**, 202001 (2015).

[3] J. A. Gordon, C. L. Holloway, A. Schwarzkopf, D. A. Anderson, S. Miller, N. Thaicharoen, and G. Raithel, Millimeter wave detection via Autler-Townes splitting in rubidium Rydberg atoms, Appl. Phys. Lett. **105**, 024104 (2014).

[4] C. L. Holloway, J. A. Gordon, S. Jefferts, A. Schwarzkopf, D. A. Anderson, S. A. Miller, N. Thaicharoen, and G. Raithel, Broadband Rydberg atom-based electric-field probe for SI-traceable, self-calibrated measurements, IEEE Trans. Antennas Propag. **62**, 6169 (2014).

[5] J. Gea-Banacloche, Y. Li, S. Jin, and M. Xiao, Electromagnetically induced transparency in ladder-type inhomogeneously broadened media: Theory and experiment, Phys. Rev. A **51**, 576 (1995).

[6] M. Fleischhauer, A. Imamoglu, and J. P. Marangos, Electromagnetically induced transparency: Optics in coherent media, Rev. Mod. Phys. **77**, 633 (2005).

[7] A. K. Mohapatra, T. R. Jackson, and C. S. Adams, Coherent optical detection of highly excited Rydberg states using electromagnetically induced transparency, Phys. Rev. Lett. **98**, 113003 (2007).

[8] M. Tanasittikosol, J. D. Pritchard, D. Maxwell, A. Gauguet, K. J. Weatherill, R. M. Potvliege, and C. S. Adams, Microwave dressing of Rydberg dark states, J. Phys. B: At. Mol. Opt. Phys. **44**, 184020 (2011).

[9] J. P. Shaffer and H. Kübler, in *Proc. SPIE Quantum Technologies* (2018), Vol. 10674.

[10] S. Kumar, H. Fan, H. Kübler, J. Sheng, and J. P. Shaffer, Atom-based sensing of weak radio frequency electric fields using homodyne readout, Sci. Rep. **7**, 42981 (2017).

[11] S. Kumar, H. Fan, H. Kübler, A. J. Jahangiri, and J. P. Shaffer, Rydberg-atom based radio-frequency electrometry using frequency modulation spectroscopy in room temperature vapor cells, Opt. Express **25**, 8625 (2017).

[12] H. Kübler, J. Keaveney, C. Lui, J. Ramirez-Serrano, H. Amarloo, J. Erskine, G. Gillet, and J. P. Shaffer, in *Proc. SPIE Optical, Opto-Atomic, and Entanglement-Enhanced Precision Metrology* (2019), Vol. 10934, pp. 1093406.

[13] M. Jing, Y. Hu, J. Ma, H. Zhang, L. Zhang, L. Xiao, and S. Jia, Atomic superheterodyne receiver based on microwave-dressed Rydberg spectroscopy, Nat. Phys. **16**, 911 (2020).

[14] M. Cai, Z. Xu, S. You, and H. Liu, Sensitivity improvement and determination of Rydberg atom-based microwave sensor, photonics **9**, 250 (2022).

[15] D. H. Meyer, K. C. Cox, F. K. Fatemi, and P. D. Kunz, Digital communication with Rydberg atoms and amplitude-modulated microwave fields, Appl. Phys. Lett. **112**, 211108 (2018).

[16] D. A. Anderson, R. E. Sapiro, and G. Raithel, An atomic receiver for AM and FM radio communication, IEEE Trans. Antennas Propag. **69**, 2455 (2021).

[17] Y. Jiao, X. Han, J. Fan, G. Raithel, J. Zhao, and S. Jia, Atom-based receiver for amplitude-modulated baseband signals in high-frequency radio communication, Appl. Phys. Express **12**, 126002 (2019).

[18] C. Holloway, M. Simons, A. H. Haddab, J. A. Gordon, D. A. Anderson, G. Raithel, and S. Voran, A multiple-band rydberg atom-based receiver: AM/FM stereo reception, IEEE Antennas Propag. Mag. **63**, 63 (2021).

[19] Z. Song, H. Liu, X. Liu, W. Zhang, H. Zou, J. Zhang, and J. Qu, Rydberg-atom-based digital communication using a continuously tunable radio-frequency carrier, Opt. Express **27**, 8848 (2019).

[20] S. M. Bohaichuk, D. Booth, K. Nickerson, H. Tai, and J. P. Shaffer, Origins of Rydberg-atom electrometer transient response and its impact on radio-frequency pulse sensing, Phys. Rev. Appl. **18**, 034030 (2022).

[21] N. Parjapati, N. Bhusal, A. P. Rotunno, S. Berweger, M. T. Simons, A. B. Artusio-Glimpse, Y. J. Wang, E. Bottomley, H. Fan, and C. L. Holloway, Sensitivity comparison of two-photon vs three-photon Rydberg electrometry, J. Appl. Phys. **134**, 023101 (2023).

[22] See Supplemental Material at http://link.aps.org/supplemental/10.1103/PhysRevApplied.20.L061004 for details of density-matrix modeling, a discussion of optimal Rabi frequencies for rf sensitivity, and effects of rf amplitude on pulse shape.

[23] N. Šibalić, J. D. Pritchard, C. S. Adams, and K. J. Weatherill, ARC: An open-source library for calculating properties of alkali Rydberg atoms, Comput. Phys. Commun. **220**, 319 (2017).

[24] A. Schwettmann, K. R. Overstreet, J. Tallant, and J. P. Shaffer, Analysis of long-range Cs Rydberg potential wells, J. Mod. Opt. **54**, 2551 (2007).

[25] C. J. H. Pagett, P. H. Moriya, R. Celistrino Teixeira, R. F. Shiozaki, M. Hemmerling, and Ph. W. Courteille, Injection locking of a low cost high power laser diode at 461 nm, Rev. Sci. Instrum. **87**, 053105 (2016).

[26] M. A. Richards, *Fundamentals of Radar Signal Processing*, 2nd ed. (McGraw-Hill, New York, 2014).

[27] F. Ripka, H. Amarloo, J. Erskine, C. Liu, J. Ramirez-Serrano, J. Keaveney, G. Gillet, H. Kübler, and J. P. Shaffer, in *Proc. SPIE Optical and Quantum Sensing and Precision Metrology* (2021), Vol. 11700.